Journal of the Korean Ceramic Society (2025) 62:1023–1029
https://doi.org/10.1007/s43207-025-00527-9

ORIGINAL ARTICLE

Thickness controlled $CsPbBr_3$ nanocrystal films for high efficiency (6% EQE) perovskite LEDs

Heeyoung Kwack[1] · Min-Seong Kim[1] · Youngjun Cho[1] · Taehoon Kim[1] · Jae-Min Myoung[1] · Wooyoung Shim[1]

Received: 28 April 2025 / Revised: 6 June 2025 / Accepted: 13 June 2025 / Published online: 30 June 2025

Abstract
Metal halide perovskite light-emitting diodes (PeLEDs) offer high color purity and tunable emission, yet device efficiency is critically dependent on the morphology of the perovskite emissive layer (EML). In this work, we systematically explore the impact of CsPbBr3 EML thickness-ranging from 15 to 56 nm-on optical and electrical performance. Films were deposited by spin coating a CsBr:$PbBr_2$ precursor in DMSO at varied speeds, followed by annealing at 100 °C. Steady-state and time-resolved photoluminescence measurements reveal that a 40 nm EML maximizes radiative recombination, exhibiting the highest PL intensity and an average lifetime of ~ 51 ns. SEM and AFM analyses confirm that 40 nm films achieve optimal grain uniformity and minimal defect density. Integrating this film into PeLEDs yields an external quantum efficiency (EQE) of 6%, surpassing devices with both thinner and thicker layers. These results establish a clear thickness-efficiency correlation and provide a practical design rule for high-performance perovskite LEDs in next-generation display technologies.

Keywords Metal halide perovskites · Grain uniformity · LED display fabrication · Charge-hole recombination efficiency

1 Introduction

Perovskite materials exhibit exceptional optoelectronic properties—most notably high optical absorption coefficients and tunable bandgaps—which have attracted intense interest for applications ranging from solar cells and displays to photodetectors and image sensors [1–4]. In particular, metal halide perovskites (MHPs) have achieved photoluminescence quantum yields (PLQYs) approaching unity (~ 100%) through advances in colloidal synthesis [5] and the strategic introduction of surface-capping ligands [6], underscoring their potential for next-generation LED displays. However, despite these breakthroughs in high-quality nanocrystal synthesis, direct integration into commercial display processes remains challenging. In industrial LED display fabrication, multilayer device architecture critically influences both photon outcoupling and power efficiency, making judicious structural design as important as the intrinsic optoelectronic properties of the perovskite [7, 8]. In particular, the thickness of the emissive layer (EML) governs charge carrier recombination dynamics and light-extraction efficiency, necessitating a thorough understanding of its impact to optimize device performance [9, 10].

In this study, we employ $CsPbBr_3$ (Fig. 1a) as the EML material. Figure 1b depicts the device architecture, which consists of: an electron injection layer (EIL) to enhance electron injection into the EML; an electron transport layer (ETL) that efficiently conveys electrons while blocking hole leakage; a hole blocking layer (HBL) to prevent holes from migrating into the ETL; the perovskite EML itself, where radiative electron–hole recombination occurs; and a hole transport layer (HTL) that shuttles holes into the EML while inhibiting electron backflow. To optimize the device structure, we systematically varied the EML thickness and assessed its impact on performance. We found that

✉ Heeyoung Kwack
hykwack@yonsei.ac.kr

Min-Seong Kim
Minseongkim@yonsei.ac.kr

Youngjun Cho
LSoo0@yonsei.ac.kr

Taehoon Kim
kthterry@yonsei.ac.kr

Jae-Min Myoung
jmmyoung@yonsei.ac.kr

Wooyoung Shim
wshim@yonsei.ac.kr

[1] Department of Materials Science and Engineering, Yonsei University, Yonsei-ro 50, Seoul 120-749, Korea

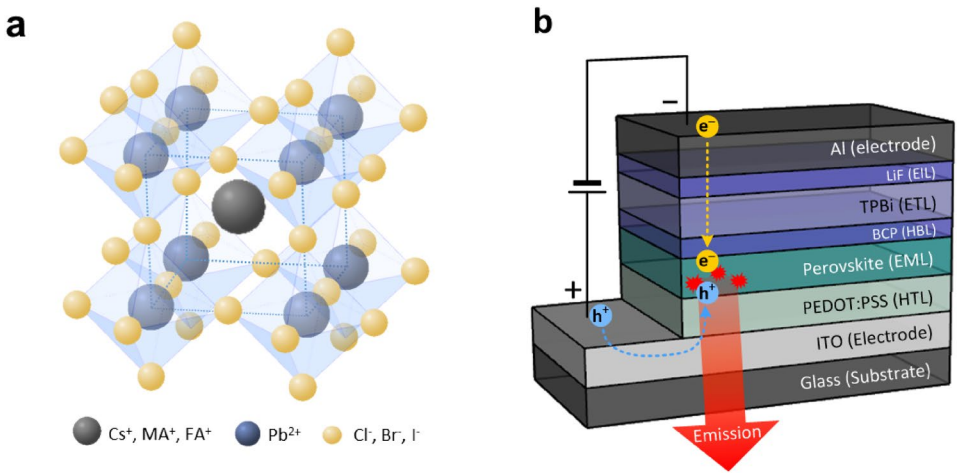

Fig. 1 Schematics of **a** Perovskite Structure and **b** Perovskite LED Device

a 40 nm $CsPbBr_3$ film exhibited superior grain uniformity and enhanced charge carrier recombination compared to thinner or thicker films, resulting in an external quantum efficiency (EQE) of approximately 6% in the fabricated perovskite LEDs.

2 Results

Perovskite LEDs function when electrons and holes, respectively injected from the cathode and anode, traverse the charge-transport layers and recombine as excitons within the perovskite EML, emitting photons at the material's bandgap energy. The more effectively electrons and holes recombine in the perovskite, the higher the device's luminous efficiency [11, 12]. Here, we optimized EML thickness to induce small, uniform $CsPbBr_3$ grains, suppress leakage through pinholes, and shorten exciton diffusion paths, thereby maximizing radiative recombination [13–16].

To assess the impact of EML thickness on device efficiency, we fabricated five perovskite LEDs with $CsPbBr_3$ emissive layers of differing thickness by varying the spin-coating speed of the precursor solution (Fig. 2a). The precursor was prepared by dissolving CsBr and $PbBr_2$ in dimethyl sulfoxide (DMSO) at a 1:1 molar ratio, followed by stirring at room temperature for 24 h to ensure full dissolution. Films were deposited by spin-coating this solution at 2000, 3000, 4000, 5000, and 6000 rpm for 60 s, yielding $CsPbBr_3$ layers of approximately 56, 40, 31, 21, and 15 nm, respectively. Finally, all samples were annealed at 100 °C for 10 min to crystallize the perovskite thin films.

To evaluate the luminescent properties of the fabricated films, we measured the photoluminescence (PL) intensity of each LED (Fig. 2b). All devices exhibit a PL peak centered at 520.6 nm. Devices with EML thicknesses up to 40 nm show comparable PL intensities, whereas the 56 nm film displays a pronounced drop in intensity. Figure 2c plots the PL full-width at half-maximum (FWHM): it remains constant for films ≤ 40 nm but broadens sharply at 56 nm, indicating that grain uniformity degrades markedly in the thicker emissive layer.

Carrier lifetimes within the $CsPbBr_3$ films were assessed by time-resolved photoluminescence (TRPL). Figure 2d shows the normalized PL decay, I(t), which we modelled with a biexponential function [17]:

$$I(t) = I_0 + A_1 e^{-t/\tau_1} + A_2 e^{-t/\tau_2} \quad (1)$$

where I_0 is the background intensity, A_1 and A_2 are the amplitudes of the fast and slow decay components, and τ_1 and τ_2 are the corresponding lifetimes. The fast time constant (τ_1) is associated with trap-mediated non-radiative recombination, while the slow time constant (τ_2) reflects radiative recombination [18]. Thus, a larger A_1:A_2 ratio indicates increased non-radiative losses, whereas a larger A_2 signifies more efficient radiative processes. The extracted values of A_1, A_2, τ_1, and τ_2 for each film thickness are summarized in Table 1.

Figure 2e plots the average fluorescence lifetime, τ_{ave}, as a function of EML thickness, where

$$\tau_{ave} = (A_1\tau_1^2 + A_2\tau_2^2)/(A_1\tau_1 + A_2\tau_2) \quad (2)$$

using the parameters extracted from the biexponential fits in Fig. 2d [19]. The 40 nm film exhibits the longest τ_{ave} of ≈51 ns. Thicker films (> 40 nm) develop larger, nonuniform grains, which lengthen exciton diffusion paths and introduce more internal defects, thereby increasing trap-mediated non-radiative recombination and shortening τ_{ave}. Conversely, thinner films (< 40 nm) yield smaller grains with higher surface-to-volume ratios, promoting non-radiative losses via grain boundary and interface recombination. These opposing effects explain the pronounced lifetime maximum at an EML thickness of 40 nm.

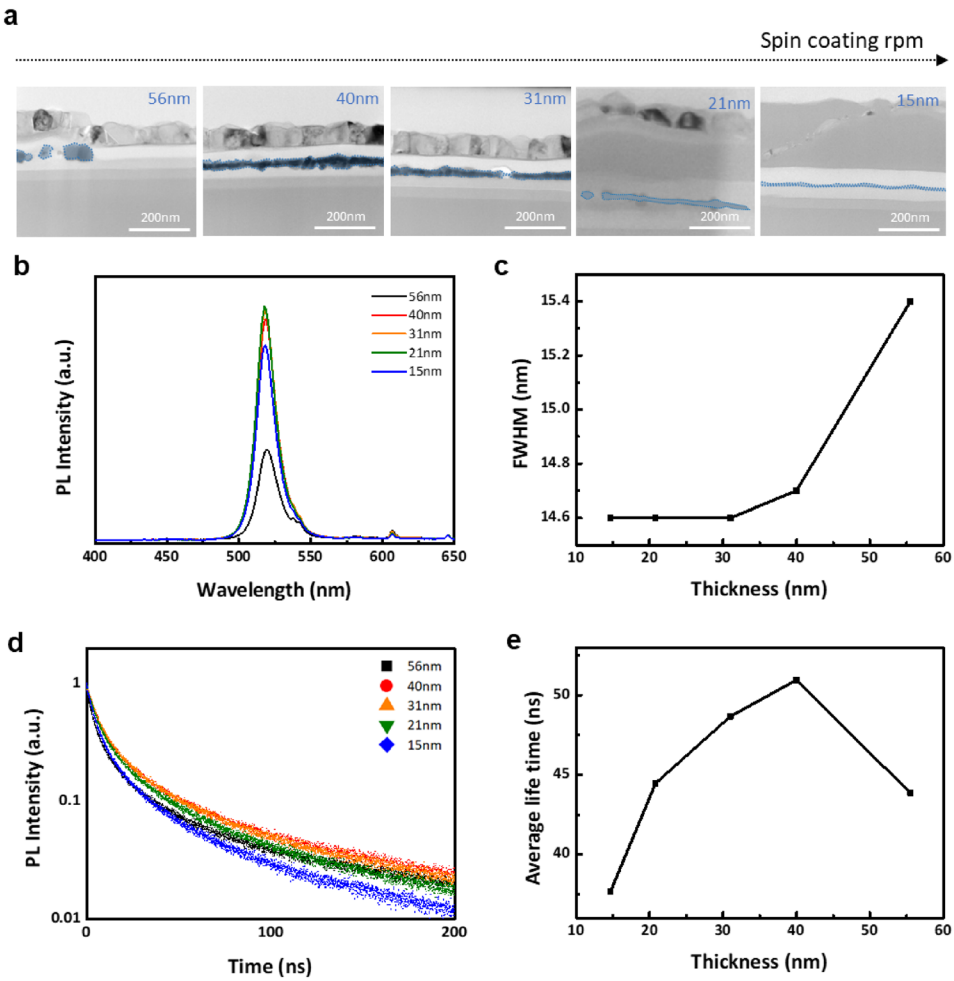

Fig. 2 **a** TEM images of perovskite thin films (blue area) at spin coating rpm of 2000, 3000, 4000, 5000, and 6000. **b** PL Intensity spectra of Perovskite EML. **c** FWHM of Perovskite EML. **d** Normalized TRPL Spectra of Perovskite EML. **e** Average lifetime of Perovskite EML

Table 1 Detailed fitting parameters of TRPL decay curves

Spin-coating speed (rpm)	Thickness (nm)	A_1	τ_1 (ns)	A_2	τ_2 (ns)	τ_{ave} (ns)
2000	56	0.83	7.4	0.17	63.9	43.9
3000	40	0.79	9.4	0.21	71.5	51.0
4000	31	0.79	9.5	0.21	69.0	48.7
5000	21	0.80	8.9	0.20	64.2	44.5
6000	15	0.84	7.9	0.16	58.7	37.7

Table 1 shows that the non-radiative amplitude coefficient A_1-attributable to defects and trap states-increases markedly whenever the EML thickness falls outside the 30–40 nm window, whereas the radiative amplitude coefficient A_2 maximizes for films in that same 30–40 nm range. These observations confirm that a spin-coated $CsPbBr_3$ EML of ≈40 nm yields the highest luminescence efficiency, with efficiency dropping off sharply for thicker layers.

To pinpoint the cause of the sharp efficiency decline in the 56 nm EML, we analyzed film morphology via SEM (Fig. 3a) and AFM (Fig. 3b). Films spun at ≥ 3000 rpm (≤ 40 nm) form uniform, densely packed grains, whereas the 2000 rpm (56 nm) coating exhibits pronounced grain aggregation, enlarged crystallites, and heterogeneous size distribution. AFM-measured root-mean-square roughness (Fig. S1) confirms that roughness begins rising even at 40 nm, reflecting the onset of aggregation. This void-rich, low-density areas introduce leakage pathways and pinholes that act as non-radiative recombination centers, undermining device performance. Such morphological degradation at excessive thickness explains the observed trend: while modestly thicker films benefit from reduced relative surface area and improved radiative efficiency, films at and

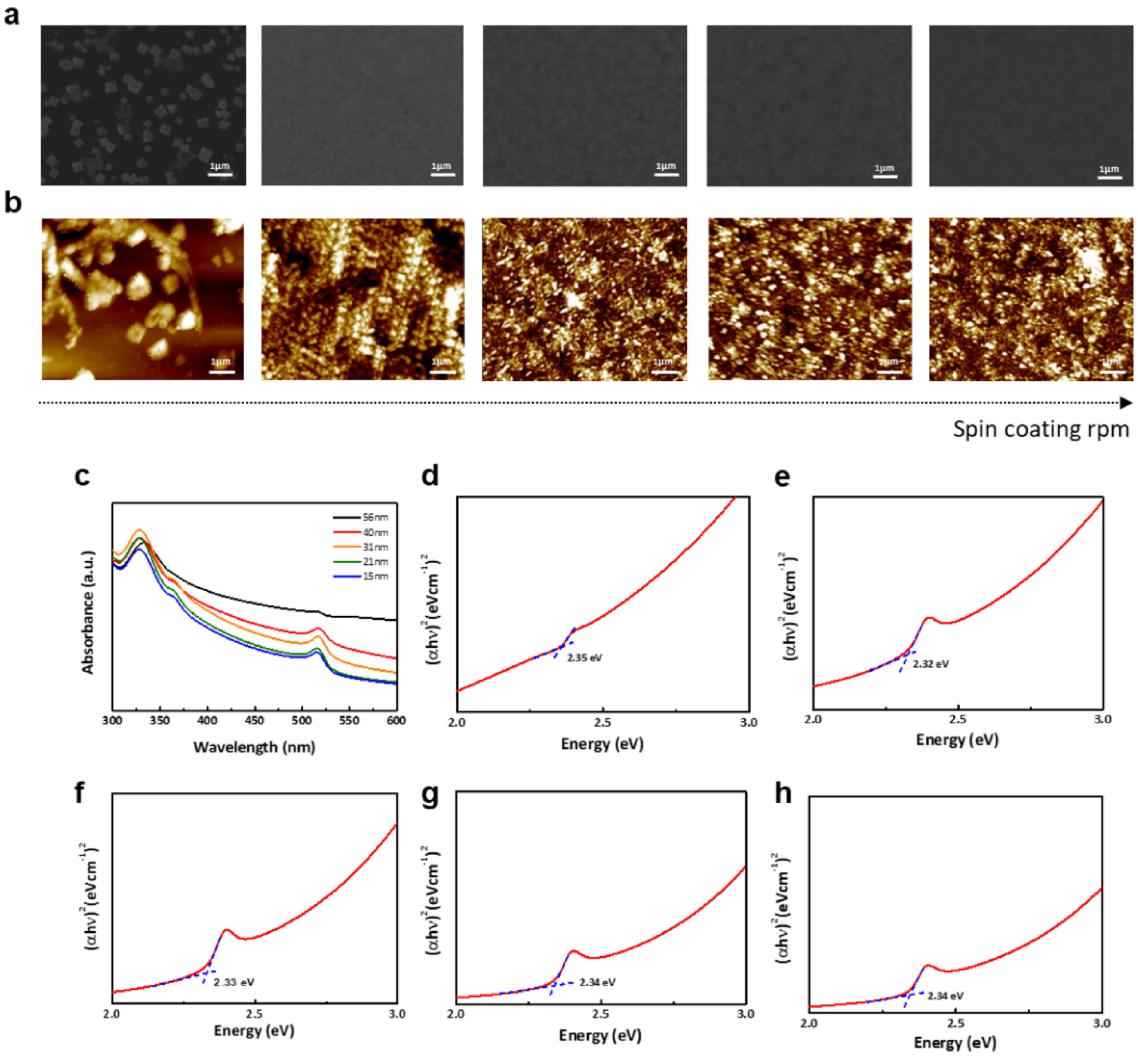

Fig. 3 **a** SEM images and **b** AFM images of perovskite thin films at spin coating rpm of 2000, 3000, 4000, 5000 and 6000. **c** Absorption of perovskite films. **d** Band gap of perovskite film at thickness of 56 nm, **e** 40 nm, **f** 31 nm, **g** 21 nm and **h**15nm

above 56 nm suffer dominating grain nonuniformity that drives the steep drop in luminescent efficiency.

Bandgaps of the five $CsPbBr_3$ films (15, 21, 31, 40, and 56 nm) were extracted from Tauc plots constructed using their UV–vis absorbance spectra (Fig. 3c). Each film shows an optical bandgap of ≈2.33 eV (Fig. 3d-h) with negligible variation, confirming that the observed differences in device efficiency and luminance arise from thickness- and morphology-driven changes in grain uniformity and film density rather than any alteration of the intrinsic band structure.

Figure 4a presents electroluminescence images of PeLEDs incorporating $CsPbBr_3$ EMLs of 15, 21, 31, 40, and 56 nm; the device with a 40 nm film shows the brightest, most uniform emission. Figure 4b shows the corresponding EL spectra under identical driving conditions: as the EML thickness decreases from 56 to 15 nm, EL intensity rises, reflecting the shorter transport path for injected electrons and holes and thus enhanced radiative recombination [20]. The current–voltage (I-V) characteristics in Fig. 4c reveal that thinner films yield lower turn-on voltages and higher current densities, indicative of more efficient carrier injection into the emissive layer [21, 22]. Similarly, the voltage-luminance (V-L) curves in Fig. 4d demonstrate that luminance increases with decreasing thickness. However, films thinner than 40 nm suffer increased interface-mediated, non-radiative recombination-diminishing EL intensity and EQE-while overly thick films (56 nm) impede carrier injection into the perovskite, also lowering recombination efficiency [23–25]. Together, these data pinpoint 40 nm as the optimal EML thickness for balancing carrier injection and radiative recombination, yielding a peak external quantum efficiency of ~ 6% (Fig. 4e).

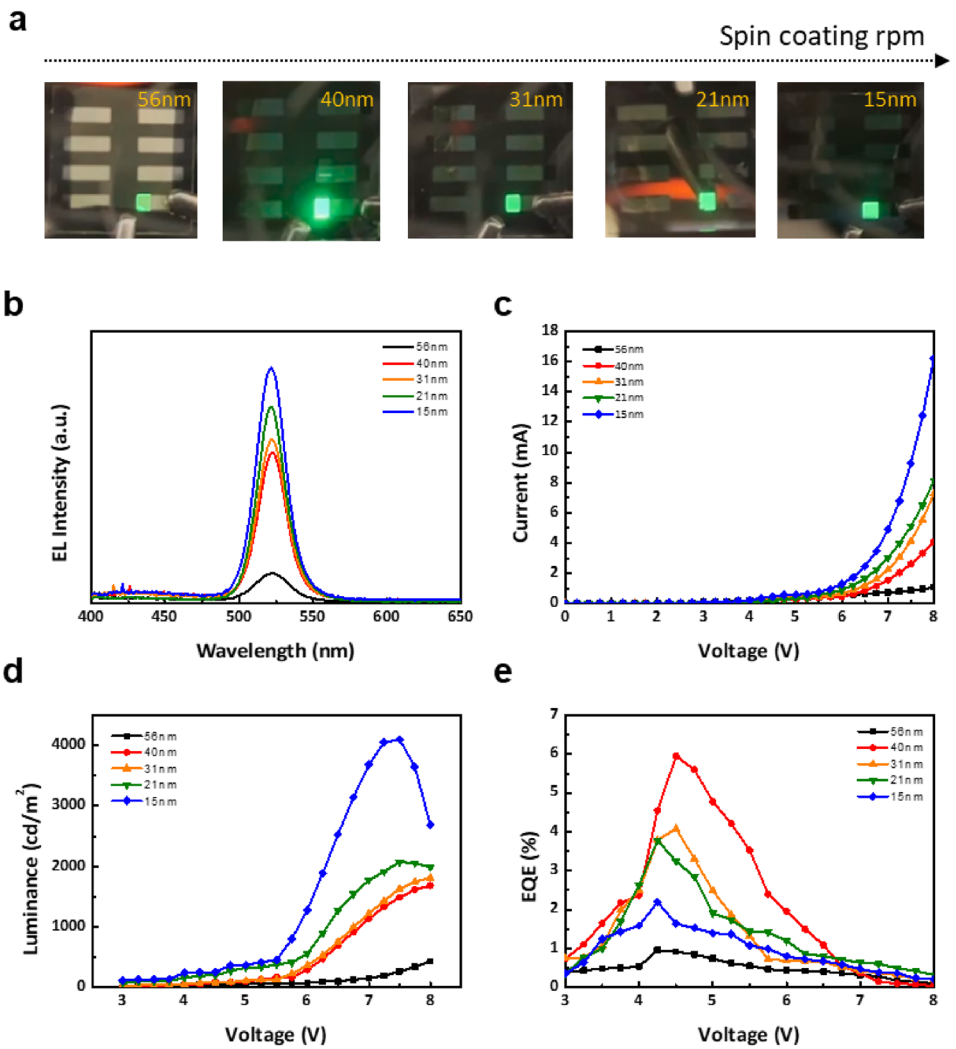

Fig. 4 **a** EML Coating images of perovskite thin films with various thickness. **b** EL Intensity, **c** Current, **d** Luminance, **e** EQE of Perovskite EML

3 Discussion

In this work, we systematically investigated how the thickness of the $CsPbBr_3$ emissive layer (EML) governs both luminance efficiency and external quantum efficiency (EQE) in perovskite LEDs. By fabricating devices with 15, 21, 31, 40, and 56 nm EMLs, we found that a 40 nm film delivers the highest EQE of 6%. At this thickness, improved film coverage and grain uniformity promote enhanced carrier injection and maximize radiative recombination within the emissive layer. Films thinner than 40 nm suffer excessive charge leakage and interface-mediated non-radiative losses, while films thicker than 40 nm incur elevated trap-induced recombination and hindered carrier injection, both of which degrade device performance.

While this study focuses on optimizing the EML thickness, it is important to recognize that the performance of perovskite LEDs is also influenced by a wide range of factors, including interfacial energy alignment, transport layer composition, and defect distribution. In addition, post-deposition strategies such as ionic doping and surface passivation have proven effective in reducing trap-assisted recombination and improving carrier dynamics. Therefore, integrating these approaches with thickness optimization may offer a more comprehensive pathway toward achieving higher efficiency and enhanced operational stability in PeLED devices. In comparison to the redesign of the structure or composition and various additional processing to improve the performance of PeLEDs, the external quantum efficiency (EQE) of about 6% achieved in this work was achieved without any omplicated methods, which is sufficiently high compared to the conventional performance of $CsPbBr_3$-based PeLEDs [26, 27]. This highlights that the thickness optimization approach in this work is effective in achieving competitive PeLED performance even with simplified device structures.

4 Method

Preparation of $CsPbBr_3$ Emissive Layers; $CsPbBr_3$ precursor solutions were prepared by dissolving CsBr and $PbBr_2$ (1:1 molar ratio) in dimethyl sulfoxide (DMSO) and stirring at room temperature for 24 h to ensure complete dissolution. Thin films of varying thickness (15, 21, 31, 40, and 56 nm) were deposited by spincoating the precursor at 6000, 5000, 4000, 3000, and 2000 rpm, respectively, for 60 s. To minimize the influence of environmental variables such as humidity and temperature during the spin-coating process and to ensure reproducibility, all perovskite thin films were fabricated under controlled conditions at a relative humidity of 30% or less and a room temperature of approximately 22 °C. All films were annealed at 100 °C for 10 min to crystallize the perovskite layer.

Device Fabrication; Indium tin oxide (ITO)-coated glass substrates were sequentially cleaned in acetone, ethanol, and deionized water (10 min each, ultrasonic bath), then treated with UV–ozone for 15 min. A thin film of PEDOT:PSS was spincoated at 4000 rpm for 60 s and annealed at 150 °C for 15 min to serve as the hole-transport layer. $CsPbBr_3$ emissive layers were then deposited under the conditions above. An electron-transport layer of ZnO nanoparticles was spincoated at 3000 rpm for 60 s and annealed at 100 °C for 10 min. Finally, aluminum electrodes (~ 100 nm) were thermally evaporated under a high vacuum.

Device Characterization; Current–voltage–luminance (J–V–L) measurements were performed using a source measure unit coupled with a calibrated photodiode to extract luminous efficacy and external quantum efficiency (EQE). Luminous efficacy was defined as the ratio of radiant flux to driving current, and EQE as the ratio of emitted photons to injected electrons. Emissive-layer thicknesses were confirmed by transmission electron microscopy (TEM) cross-section imaging.

Supplementary Information The online version contains supplementary material available at https://doi.org/10.1007/s43207-025-00527-9.

Declarations

Conflict of interests Author Kwack. H. Y has received research support from the Company LG Display. All other authors have no relevant financial or non-financial interests to disclose. The authors declare they have no financial interests.

References

1. J.J. Yoo, G. Seo, M.R. Chua, T.G. Park, Y. Lu, F. Rotermund, Y.-K. Kim, C.S. Moon, N.J. Jeon, J.-P. Correa-Baena, V. Bulović, S.S. Shin, M.G. Bawendi, J. Seo, Efficient perovskite solar cells via improved carrier management. Nature **590**, 587–593 (2021)
2. C. Zou, C. Chang, D. Sun, K.F. Böhringer, L.Y. Lin, Photolithographic patterning of perovskite thin films for multicolor display applications. Nano Lett. **20**, 3710–3717 (2020)
3. Y. He, M. Petryk, Z. Liu, D.G. Chica, I. Hadar, C. Leak, W. Ke, I. Spanopoulos, W. Lin, D.Y. Chung, B.W. Wessels, Z. He, M.G. Kanatzidis, CsPbBr3 perovskite detectors with 14% energy resolution for high-energy γ-rays. Nat. Photonics **15**, 36–42 (2021)
4. J. Jang, Y.-G. Park, E. Cha, S. Ji, H. Hwang, G.G. Kim, J. Jin, J.-U. Park, 3D heterogeneous device arrays for multiplexed sensing platforms using transfer of perovskites. Adv. Mater. **33**, 2101093 (2021)
5. Y.-H. Kim, J. Park, S. Kim, J.S. Kim, H. Xu, S.-H. Jeong, B. Hu, T.-W. Lee, Exploiting the full advantages of colloidal perovskite nanocrystals for large-area efficient light-emitting diodes. Nat. Nanotechnol. **17**, 590–597 (2022)
6. Q. Zhong, M. Cao, Y. Xu, P. Li, Y. Zhang, H. Hu, D. Yang, Y. Xu, L. Wang, Y. Li, X. Zhang, Q. Zhang, L-type ligand-assisted acid-free synthesis of CsPbBr3 nanocrystals with near-unity photoluminescence quantum yield and high stability. Nano Lett. **19**, 4151–4157 (2019)
7. H.J. An, S.D. Baek, D.H. Kim, J.-M. Myoung, Energy and charge dual transfer engineering for high-performance green perovskite light-emitting diodes. Adv. Func. Mater. **32**, 2112849 (2022)
8. Y. Lu, Z. Wang, J. Chen, Y. Peng, X. Tang, Z. Liang, F. Qi, W. Chen, Tuning hole transport layers and optimizing perovskite films thickness for high efficiency CsPbBr3 nanocrystals electroluminescence light-emitting diodes. J. Lumin. **234**, 117952 (2021)
9. H. Lee, D. Gelija, U. Kim, J. Lee, W.J. Chung, Compositional study of borosilicate CsPbBr3 perovskite nanocrystals embedded glass for chemically stable white LEDs. J. Korean Ceram. Soc. **61**, 482–491 (2024)
10. L. Zhao, K.M. Lee, K. Roh, S.U.Z. Khan, B.P. Rand, Improved outcoupling efficiency and stability of perovskite light-emitting diodes using thin emitting layers. Adv. Mater. **31**, e1805836 (2019)
11. Z. Guan, Y. Li, Z. Zhu, Z. Zeng, Z. Chen, Z. Ren, G. Li, S.-W. Tsang, H.-L. Yip, Y. Xiong, C.-S. Lee, High-efficiency blue perovskite light-emitting diodes with improved photoluminescence quantum yield via reducing trap-induced recombination and exciton-exciton annihilation. Adv. Func. Mater. **32**, 2203962 (2022)
12. G.K. Grandhi, H.J. Kim, N.S.M. Viswanath, H.B. Cho, J.H. Han, S.M. Kim, W.B. Im, Strategies for improving luminescence efficiencies of blue-emitting metal halide perovskites. J. Korean Ceram. Soc. **58**, 28–41 (2021)
13. Y. Shen, K.-C. Shen, Y.-Q. Li, M. Guo, J. Wang, Y. Ye, F.-M. Xie, H. Ren, X. Gao, F. Song, J.-X. Tang, Interfacial potassium-guided grain growth for efficient deep-blue perovskite light-emitting diodes. Adv. Func. Mater. **31**, 2006736 (2021)
14. X. Yang, H. Gu, S. Li, J. Li, H. Shi, J. Zhang, N. Liu, Z. Liao, W. Xu, Y. Tan, Improved photoelectric performance of all-inorganic perovskite through different additives for green light-emitting diodes. RSC Adv. **9**, 34506–34511 (2019)
15. X. Cheng, C. Qi, W. Ding, J. Lu, X. Mo, Y. Zhou, T. Lin, X. Tao, H. Chen, Y. Ouyang, Boosted electroluminescence of perovskite light-emitting diodes by pinhole passivation with insulating polymer. J. Phys. D Appl. Phys. **51**, 405103 (2018)
16. S.-D. Baek, W. Shao, W. Feng, Y. Tang, Y.H. Lee, J. Loy, W.B. Gunnarsson, H. Yang, Y. Zhang, M.B. Faheem, P.I. Kaswekar, H.R. Atapattu, J. Qin, A.H. Coffey, J.Y. Park, S.J. Yang, Y.-T. Yang, C. Zhu, K. Wang, K.R. Graham, F. Gao, Q. Qiao, L.J. Guo, B.P. Rand, L. Dou, Grain engineering for efficient near-infrared perovskite light-emitting diodes. Nat. Commun. **15**, 10760 (2024)
17. P. Sadhukhan, M.S. Kim, J.-M. Myoung, Synergetic mixed ionic liquid strategy for comprehensive defect passivation and increased carrier mobility in high-performance green perovskite light-emitting diodes. Chem. Eng. J. **480**, 148186 (2024)

18. C. Liu, Y. Liu, S. Wang, J. Liang, C. Wang, F. Yao, W. Ke, Q. Lin, T. Wang, C. Tao, G. Fang, Highly efficient quasi-2d green perovskite light-emitting diodes with bifunctional amino acid. Adv Opt Mater **10**, 2200276 (2022)
19. Kim, M. S., Sadhukhan, P. & Myoung, J. M. High-performance blue perovskite films and micro-arrays for light-emitting diodes with ionic liquid interlayer. *Advanced Functional Materials* **34**, (2024).
20. D.-H. Kang, S.-G. Kim, Y.C. Kim, I.T. Han, H.J. Jang, J.Y. Lee, N.-G. Park, CsPbBr3/CH3NH3PbCl3 double layer enhances efficiency and lifetime of perovskite light-emitting diodes. ACS Energy Lett. **5**, 2191–2199 (2020)
21. Y.-J. Jung, S.-Y. Cho, J.-W. Jung, S.-Y. Kim, J.-H. Lee, Influence of indium-tin-oxide and emitting-layer thicknesses on light outcoupling of perovskite light-emitting diodes. Nano Convergence **6**, 26 (2019)
22. V. Prakasam, F. Di Giacomo, R. Abbel, D. Tordera, M. Sessolo, G. Gelinck, H.J. Bolink, Efficient perovskite light-emitting diodes: effect of composition, morphology, and transport layers. ACS Appl. Mater. Interfaces **10**, 41586–41591 (2018)
23. J.-H. Park, H.-R. Kim, M.-J. Kang, D.H. Son, J.-C. Pyun, Trends in defect passivation technologies for perovskite-based photosensor. J. Korean Ceram. Soc. **61**, 15–33 (2024)
24. Z. Li, K. Cao, J. Li, X. Du, Y. Tang, B. Yu, Modification of interface between PEDOT:PSS and perovskite film inserting an ultrathin LiF layer for enhancing efficiency of perovskite light-emitting diodes. Org. Electron. **81**, 105675 (2020)
25. C. Liu, B. Li, M. Qiu, Advancements in the improvement of optical outcoupling efficiency for perovskite LEDs. Adv Devices Instrum **5**, 0045 (2024)
26. S.-R. Bae, M.J. Seol, S.Y. Kim, CsPbBr3 and Cs4PbBr6 perovskite light-emitting diodes using a thermally evaporated host–dopant system. Nanoscale **15**, 9533–9542 (2023)
27. L.-C. Chen, C.-H. Kao, Improved extraction efficiency of CsPbBr3 perovskite light-emitting diodes due to anodic aluminum oxide nanopore structure. Sci. Rep. **12**, 14750 (2022)